

# Laser Production of Extreme Ultraviolet Light Source for the Next Generation Lithography Application<sup>\*)</sup>

Shinsuke FUJIOKA, Hiroaki NISHIMURA, Katsunobu NISHIHARA, Noriaki MIYANAGA, Yasukazu IZAWA, Kunioki MIMA, Yoshinori SHIMADA<sup>1)</sup> and Atsushi SUNAHARA<sup>1)</sup>

*Institute of Laser Engineering, Osaka University, 2-6 Yamada-oka, Suita, Osaka, Japan*

<sup>1)</sup>*Institute for Laser Technology, 2-6 Yamada-oka, Suita, Osaka, Japan*

(Received 25 August 2008 / Accepted 24 August 2009)

Extreme ultraviolet lithography (EUVL) is a technology to be used in mass production of the next-generation semiconductor devices. Critical issues in the development of a Sn-based EUV source are in achieving a high conversion efficiency (CE) of incident laser energy into EUV light, reducing debris emanating from light source plasmas, and suppressing out-of-band radiation beside the EUV light. The minimum-mass target, which contains the minimum number of Sn atoms required for sufficient EUV radiation, is a solution to these critical issues. One practical-minimum mass target is a pure Sn microdroplet. Laser-driven expansion of a pure Sn microdroplet is proposed to solve the considerable mismatch between the optimal laser spot diameter (300  $\mu\text{m}$ ) and the diameter (20  $\mu\text{m}$ ) of microdroplets containing the minimum-mass Sn fuel for generating the required EUV radiant energy (10 mJ/pulse). An expanded microdroplet was irradiated with a CO<sub>2</sub> laser pulse to generate EUV light. A combination of low density and long scale length of the expanded microdroplet leads to a higher EUV energy CE (4%) than that (2.5%) obtained from planar Sn bulk targets irradiated by a single CO<sub>2</sub> laser pulse. This scheme can be used to produce a practical EUV light source system with an EUV CE of 3.9%.

© 2009 The Japan Society of Plasma Science and Nuclear Fusion Research

Keywords: extreme ultraviolet light, laser-produced plasma, x-ray radiation source

DOI: 10.1585/pfr.4.048

## 1. Introduction

Extreme ultraviolet (EUV) light sources for lithography are being investigated intensively as an attractive application for laser-produced plasmas (LPPs) in industry [1]. Radiation of 13.5 nm wavelength within a 2% bandwidth has been selected as suitable EUV radiation for lithography because a Mo/Si multilayer mirror has the highest reflectivity ( $\sim 70\%$ ) for the in-band light. Laser-produced tin (Sn) plasma has a high-intensity emission peak at 13.5 nm; thus, much effort is being devoted in developing a Sn-based EUV light source [2–9]. Some critical issues in the development of a Sn-based EUV source include achieving a high conversion efficiency (CE) of incident laser energy into in-band light, reducing debris emanating from light source plasmas, and suppressing out-of-band (OOB) light in the vacuum ultraviolet region. The use of a minimum-mass target [10, 11], which contains the minimum number of Sn atoms required for EUV radiant energy is a solution to achieve these goals. This paper consists of eight sections; the experimental setup is summarized in Sec. 2, minimum-mass Sn fuel for sufficient EUV radiation is discussed in Sec. 3 [10–12], reduction of neutral debris emanation is demonstrated [12, 13] in Sec. 4, suppression of OOB radiation is demonstrated [14, 15] in

Sec. 5, practical EUV light source generation with a pure Sn microdroplet [16] is described in Sec. 6, and a practical design of an EUV light source system is discussed [16] in Sec. 7. Section 8 is the summary of the paper.

## 2. Experimental Setup

Sn plasmas were generated with a single-shot operated 10-Hz Nd:YAG laser (1.064  $\mu\text{m}$  of wavelength) excepting the experiment described in Sec. 6. Two types of laser pulse were used, one is a 2.5 ns Gaussian-shaped pulse and the other an 8.0 ns Gaussian-shaped pulse. Pulse duration, average intensity, spot diameter and energy of the shorter pulse were 2.5 ns of FWHM,  $1 \times 10^{11}$  W/cm<sup>2</sup>, 500  $\mu\text{m}$  and 0.5 J/pulse, respectively. These values are the optimum conditions for EUV generation with a Nd:YAG laser [8]. The corresponding values of the longer pulse were 8.0 ns of FWHM,  $1 \times 10^{11}$  W/cm<sup>2</sup>, 500  $\mu\text{m}$  and 1.6 J/pulse, respectively. The laser incident axis was normal to the target surface.

Four types of targets were used; a planar Sn bulk of 250  $\mu\text{m}$  in thickness (called bulk), a thin Sn layer coated on a plastic plate (called all-coat), a thin Sn dot coated on a glass plate (called dot), and a thin Sn layer coated on a plastic sphere (called sphere). The diameter of the dots and spheres was 500  $\mu\text{m}$  that was equal to the Nd:YAG laser spot diameter.

author's e-mail: sfujioka@ile.osaka-u.ac.jp

<sup>\*)</sup> This article is based on the invited talk at the 14th International Congress on Plasma Physics (ICPP2008).

EUV spectra were obtained with a grating spectrometer and a cooled back-illumination x-ray charge-coupled-device (CCD) camera. Absolute EUV energy was measured with a calibrated EUV energy monitor (E-MON of Jenoptik [17]). The E-MON consists of an aperture, a pair of Mo/Si multilayer mirrors, a Zr filter, and an x-ray photo diode. To determine the angular distribution of EUV emission, x-ray photodiodes were arranged at 30, 60, 75, and 90 degrees relative to the target normal. These diodes were coated with a 350-nm-thick Mo layer and a 500-nm-thick Si layer; these layers function as a band-pass filter for 13.5-nm radiation. The diodes were calibrated using the E-MON. The signal of the E-MON and photodiodes were recorded with a 1-GHz oscilloscope.

### 3. Minimum Mass of Sn Fuel for Sufficient EUV Radiant Energy

The opacity, as well as the emissivity, of laser-produced Sn plasma is so high for 13.5 nm light that the light emitted from deep within the Sn plasma is absorbed strongly by the surrounding plasma. The opacity of a uniform Sn plasma produced by thermal radiation confined in a laser-heated gold cavity was measured for evaluating quantitatively the opacity effects on EUV CE [5]. The experimental result reveals that laser energy transported into target layers deeper than 10 nm is not efficiently converted into 13.5 nm light, and therefore only a thin Sn layer below 10 nm should be heated by a laser pulse, yielding efficient EUV emission [5].

The minimum number of Sn atoms for sufficient EUV emission was evaluated by measuring EUV-CEs with changing target thickness and geometries. Figure 1 shows the dependence of CEs on the shapes and thicknesses

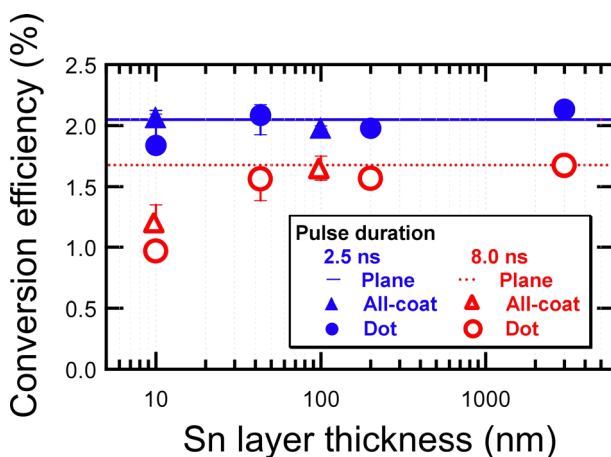


Fig. 1 Dependence of CEs on the shapes and thicknesses of Sn targets. The triangular and circular points represent CEs for the all-coat and dot targets irradiated with an 8.0-ns-(open) and 2.5-ns-(closed) laser pulse, respectively. The solid and dashed lines indicate CEs obtained from the bulk target with 2.5 and 8.0 ns pulse durations.

of Sn targets. The triangular and circular points represent CEs for the all-coat and dot targets irradiated by an 8.0 ns (open) and 2.5 ns (closed) laser pulse. The solid and dashed lines indicate CEs obtained with the bulk targets irradiated by a 2.5 and 8.0 ns pulse for comparison. With decrease in the coating thickness, CEs keep the same value for the bulk target down to 10-nm-thickness for 2.5 ns laser pulse. It was found that the Sn atoms located out of the laser spot do not contribute to the EUV emission.

The number of Sn atoms contained inside the dot diameter (500  $\mu\text{m}$ ) and the 10 nm of thickness is  $7.3 \times 10^{13}$ , and radiant energy of in-band light is 10.5 mJ, which corresponds to  $7.1 \times 10^{14}$  photons. Therefore each Sn atom emits 9.8 photons/atom of in-band light. Similar calculation has been done for an 8.0 ns pulse, and the photon number per Sn atom is evaluated to be 5.4 photons/atom.

### 4. Reduction of Neutral Debris with Minimum Mass Target

Sn is a condensable material, thus Sn debris emanating from source plasmas contaminate the first EUV collection mirror that is placed close to the plasma source. Merely 1-nm-thick deposition of a solid Sn layer on the mirror reduces its reflectivity by 10%, thus Sn debris must be minimized. Debris from source plasma consist of ions and neutral particles (atoms, clusters, droplets, etc.). An electromagnetic field can be applied to shield the first EUV collection mirror from ions bombardment, however the neutral particles are hardly blocked. The absolute number and spatial distribution of the neutral atomic debris from the minimum-mass targets were selectively and quantitatively measured by means of a laser-induced-fluorescence (LIF) technique [18].

LIF is an optical emission from atoms excited from a certain level to upper levels due to the resonance absorption of laser light. The excited atoms deexcite and emit a certain wavelength light inherent in the atom. Atomic species and ionization states can be selected by adjusting the wavelength and spectral width of the probe laser light. In the experiment, a second harmonics of a dye laser using Rhodamine 6G, i.e., 286.33 nm wavelength, was used as the probe laser to excite the neutral atomic debris from the ground state ( $5p^2 \ ^3P_0$ ) to the upper state ( $6s \ ^3P_1$ ), and corresponding fluorescence at 317.5 nm via  $6s \ ^3P_1 - 5p^2 \ ^3P_2$  transition was observed. To observe the cross section of neutral Sn plumes, the probe light was focused to a sheet beam shape (150  $\mu\text{m}$  thickness  $\times$  1.1 cm width) by a cylindrical lens, and was incident from the side of the target. Pulse duration and intensity of the dye laser were 10 ns and  $2 \times 10^7 \text{ W/cm}^2$ , respectively. Dependence of the fluorescence intensity on the number of an object atom was experimentally obtained by comparing the LIF intensity with the density of neutral atomic debris that was measured in a separate experiment with an EUV backlight technique [19]. The fluorescence intensity was found to be linearly pro-

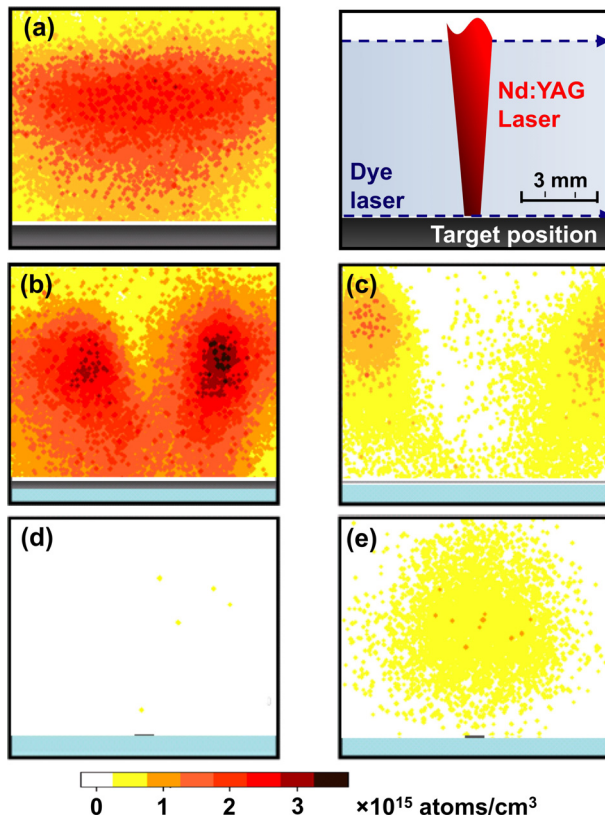


Fig. 2 Laser-induced-fluorescence images, showing spatial distributions of the neutral atomic debris for (a) bulk, (b) 100-nm-thick all-coat, (c) 10-nm-thick all-coat, (d) 10-nm-thick dot, and (e) 3000-nm-thick dot targets. Images were taken at  $1.0 \mu\text{s}$  after Nd:YAG laser irradiation. The pulse duration of the Nd:YAG laser was 2.5 ns.

portional to the density of neutral atomic Sn debris under our experimental conditions, and the proportionality constant ( $=1.16 \times 10^{-2}$  photons/atom) was obtained by a linear fitting.

Figure 2 shows LIF images for the bulk, the 100-nm and 10-nm-thick all-coat, and the 3000-nm and 10-nm-thick dot targets. These were taken at  $1.0 \mu\text{s}$  after Nd:YAG laser irradiation, whose pulse duration was 2.5 ns. Fluorescence intensity and spatial extension of the neutral atomic Sn debris are drastically changed for different types of targets. The spatial distribution for a bulk target is relatively uniform as shown in Fig. 2(a). In the all-coat target cases (Figs. 2(b) and 2(c)), LIF images have a dip along the laser incident axis. These experimental results indicate that Sn atoms in the laser spot are highly ionized, whereas those in the periphery of the laser spot are weakly heated via heat conduction and radiations from the hot plasma. Thus, Sn atoms in the periphery are emitted as low-charged ions and/or neutral debris. In the 10-nm dot target case (Fig. 2(d)), all of the Sn atoms were ionized, and signal was the noise-level. Ablation depth was evaluated to be 10 nm with the present laser conditions [10]. The Sn targets of 100 nm and 3000 nm thickness are much thicker

Table 1 Total amount of neutral atomic Sn debris emanated from the various targets.

Target geometry	Total amount of neutral Sn atomic debris
Bulk	$3.5 \times 10^{15}$
100 nm-thick all-coat	$1.7 \times 10^{16}$
10 nm-thick all-coat	$6.9 \times 10^{14}$
3000 nm-thick dot	$6.3 \times 10^{15}$
43 nm-thick dot	$4.8 \times 10^{13}$

than the ablation depth. Therefore, Sn atoms in deeper region were emitted as neutral atomic debris as shown in Figs. 2 (b) and 2 (e).

The total amount of neutral atomic debris was calculated by taking the expansion velocity into consideration. The total amount of neutral atomic debris from the 43-nm-thick dot target was only 1.37% of that from the bulk target in the case of 2.5 ns laser pulse duration. This evaluation was summarized in Table 1.

It is recognized in the EUV lithography community that the power of an EUV light source should maintain more than 90% of its initial value during at least a half year. Merely 1-nm-thick deposition of a solid Sn layer on the mirror reduces its reflectivity by 10%. Suppose all the emitted neutral debris is deposited on a Mo/Si mirror set 10 cm away from the plasma. This results in the mirror being coated with a 1-nm-thick Sn layer only after  $5 \times 10^5$  shots with the 43-nm dot target and Nd:YAG laser, i.e. 10 s under 50 kHz operation, which is  $6.3 \times 10^{-7}$  times shorter than the requirement. Even though additional mitigation and removal schemes for the Sn contamination are required, supply of the minimum mass target is the essential issue for an Sn-based EUV light source. Note that if Sn bulk was irradiated with a  $\text{CO}_2$  laser, the amount of neutral atomic Sn debris is 0.2% of that with a Nd:YAG laser. Further mitigation of Sn debris is definitely realized by coupling the  $\text{CO}_2$  laser with the minimum-mass target.

## 5. Suppression of Out-of-Band Radiation with the Minimum Mass Target

The EUV exposure system includes several (typically 6 or 8) Mo/Si multilayer mirrors [20], each of which has high reflectivity not only for in-band light but also for OOB light, at wavelengths longer than 130 nm. Such OOB radiation can range across the spectrum from vacuum ultraviolet (VUV) to infrared (IR) [1], seriously degrading EUVL performance. OOB light is generally classified into two bands, the first from 130 to 400 nm (VUV/ultraviolet (UV)), and the second from 400 nm through the infrared (visible (VIS)/IR). Transmitted VUV/UV radiation on the

photoresist material causes local flares on the wafer, while VIS/IR radiation can deform the optics, reticle, and wafers due to the resulting heat load. According to the joint requirements announced in May 2006, the VUV/UV and VIS/IR radiant energies must be less than 7% and 3% of the in-band light energy, respectively, at the intermediate focus (IF) point, which is the entrance of the EUV projection system from the EUV light source system. Spectra [21] and angular distributions [22] of OOB radiation were previously measured in the wavelength range from 200 nm to IR. In the present study, the absolute energy, spectra, and angular distributions were measured in the VUV/UV range (130 - 400 nm), which is the dominant component of OOB radiation.

In this study, a transmission grating spectrometer (TGS) was used to measure the absolute OOB spectra and energy. A TGS was chosen because of its stable spectral response. The TGS was made on a 5- $\mu\text{m}$ -thick nickel substrate. Its grating pitch was 10  $\mu\text{m}$  with a periodic combination of spaces and bars 5  $\mu\text{m}$  wide. The OOB spectrum was recorded with a back-illumination-type CCD. The TGS provides spatial resolution along the direction perpendicular to the dispersion axis. The field of view of the TGS system was 5 mm, the spectral resolution was 20 nm, and the spatial resolution was 600  $\mu\text{m}$  for 130 nm light [23]. The spectral responses of the TG and the CCD in the VUV/UV range were calibrated as described below.

The diffraction efficiency of an optical grating depends on the photon energy, grating material, substrate, thickness, and line/space ratio [24]. The spectral response of the CCD was measured in the VUV range from 130 nm to 200 nm, because a thin contamination layer on the CCD surface strongly affects the response in this region. VUV synchrotron orbital radiation from beam line "5B" of the UVSOR facility at the Institute for Molecular Science (Okazaki, Japan) was used for the CCD calibration. A 5-mm-thick  $\text{CaF}_2$  window was inserted to filter out higher order light (shorter than 130 nm). The energy of the resulting monochromatic light was measured using a calibrated photodiode. The obtained response curve agrees well with calculations [25] assuming an analog-to-digital converter gain of 1.9 electrons/count and the commercially published quantum efficiency of the CCD.

After the calibration, we collected absolute VUV spectra from laser-produced Sn plasmas. Initially the angular distribution of the OOB radiation was measured using a GaP photodiode covered with a 1-mm-thick  $\text{CaF}_2$  window. The absolute OOB radiant energy was evaluated by taking these distributions into account. For the spherical targets, the spatial extent of the VUV/UV emission is equal to that of the laser spot size, while it is about twice the laser spot size for the planar targets. Therefore OOB radiation is generated not only within the laser spot but also in its periphery heated by electron thermal conduction and by radiation from the high-temperature EUV emission region.

Figure 3 shows measured OOB spectra integrated over

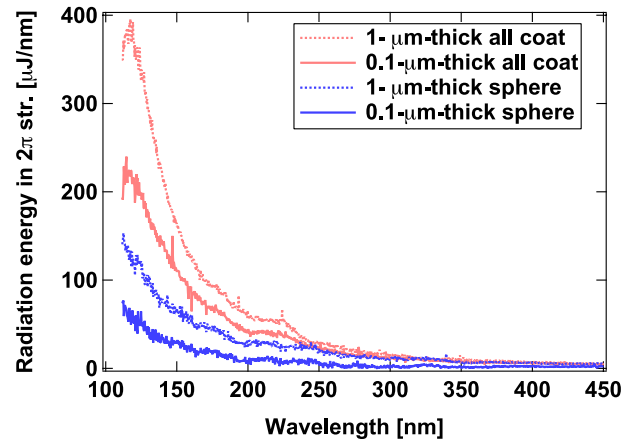


Fig. 3 Measured OOB spectra (130 - 400 nm wavelengths) for a 2 ns laser pulse. The targets were 1- $\mu\text{m}$ - and 0.1- $\mu\text{m}$ -thick Sn planes and spheres.

Table 2 Percentage ratios of the out-of-band to in-band radiation under various target and laser conditions. These were evaluated at the source point.

Target geometry	OOB/IB radiation (%)
Bulk	173 $\pm$ 12.0
1- $\mu\text{m}$ -thick plane	180 $\pm$ 9.0
0.1- $\mu\text{m}$ -thick plane	115 $\pm$ 4.0
10-nm-thick plane	55.6 $\pm$ 5.4
1- $\mu\text{m}$ -thick sphere	63.8 $\pm$ 3.3
0.1- $\mu\text{m}$ -thick sphere	40.3 $\pm$ 6.1

the entire OOB emission region for a 2-ns pulse duration. OOB radiation from the periphery of the laser spot was suppressed in energy by 75 - 80% for spherical targets compared to all-coat targets. Also, the OOB radiation emanating from a 0.1- $\mu\text{m}$ -thick Sn all-coat target is 40 - 50% of that from a 1- $\mu\text{m}$ -thick all-coat target, indicating that some OOB radiation is emitted from deep inside the EUV source plasma. Consequently an optically thin plasma would reduce the OOB radiation. The spectra were fitted to Planck curves, resulting in radiation temperatures in the range of 4 to 7 eV. Therefore, the OOB radiative region has a relatively low temperature in comparison with the EUV emissive region temperature (typically 20 - 50 eV) [1].

Table 2 summarizes the ratio of the OOB to in-band radiation for various target and laser conditions. The smallest fraction of OOB radiation was obtained for a 2-ns pulse and a 0.1- $\mu\text{m}$ -thick spherical target. OOB radiation can be reduced, while keeping the in-band radiation efficiency high, by limiting both the fuel size within the laser spot and the supplied fuel mass.

The OOB radiant energy in the 130 - 400 nm band at the IF point was evaluated using the spectral reflectivity of the Mo/Si mirror. The spectrum for the best case in Ta-

ble I was used in this evaluation. The OOB radiant energy integrated from 130 to 400 nm is 1.38 mJ at the IF point, compared to 3.12 mJ at the source location, for an incident laser pulse energy of 300 mJ. Thus the effective reflectivity of the Mo/Si mirror in the 130 - 400 nm range is found to be 44.2%. The energy of the OOB light is 26.4% of the in-band energy (5.22 mJ) at the IF point. Although this value does not satisfy the joint requirement, a guiding principle to reduce the OOB radiation was clarified in this study.

When Sn bulk was irradiated with a CO<sub>2</sub> laser, the OOB radiant energy (integrated from 130 to 400 nm) from the CO<sub>2</sub> laser-produced tin plasmas was 4.8% of that with the Nd:YAG laser. The energy of the UV/VUV light was 8.65% of the in-band energy at the IF point, which is slightly larger than the joint requirement. On the other hand, radiation-hydrodynamic simulation predicts only half of incident CO<sub>2</sub> laser energy is absorbed in a Sn plasma [29], which implies that reflected and scattered CO<sub>2</sub> laser light may be a crucial source of OOB radiation in the IR range, while such light is not significant for Nd:YAG lasers.

## 6. Optimal EUV Light Source Generation with Microdroplet

An EUV power of 180 W is required at the IF point to achieve EUV lithography [1]. About 33% of the EUV radiation emitted from the source plasma can be transported to the IF point [1]. Thus, a practical EUV light source requires 545 W of EUV power in  $2\pi$  sr. Assuming a repetition rate of 50 kHz for EUV light radiation generation, the in-band radiant energy must be 10.9 mJ/pulse, which corresponds to  $7.4 \times 10^{14}$  photons/pulse. In a laser-produced plasma, Sn ions emit in-band photons while traveling from the target surface through the high-temperature, low-density corona region. The number of in-band photons emitted per Sn ion was measured to be in the range of 5 to 10 as discussed in Sec. 3. Therefore, the minimum number of Sn atoms for the required EUV radiant energy is evaluated to be in the range of  $7.4 \times 10^{13}$  to  $1.5 \times 10^{14}$ . This number of Sn atoms is contained in a pure Sn microdroplet with a diameter of 20  $\mu\text{m}$ . A CO<sub>2</sub> laser (wavelength: 10.6  $\mu\text{m}$ ) is a practical driver for efficient EUV light source production [6, 26], because CO<sub>2</sub> laser-produced Sn plasma is optically thin for the in-band radiation so that self-absorption of the in-band radiation is negligibly small in the plasma [5]. The optimal intensity and pulse duration of a CO<sub>2</sub> laser were assumed to be  $1 \times 10^{10}$  W/cm<sup>2</sup> and 40 ns, respectively, and the EUV-CE was taken to be 4% (details are discussed below), so that the energy in a single laser pulse will be 273 mJ/pulse. To obtain this optimal laser intensity, the laser spot diameter must be 295  $\mu\text{m}$ . This simple evaluation indicates that the diameter (20  $\mu\text{m}$ ) of the minimum-mass droplet is too small to be irradiated by the optimal laser intensity ( $1 \times 10^{10}$  W/cm<sup>2</sup>) and required laser energy (273 mJ). To resolve this considerable

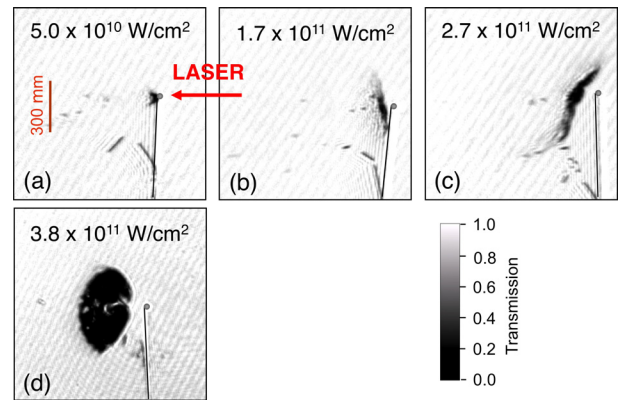


Fig. 4 Side-on shadowgraphs of expanded microdroplets were taken 0.5  $\mu\text{s}$  after the laser irradiation. The artificial shadows indicate the initial position and shape of the droplet. Laser intensities were (a)  $5.0 \times 10^{10}$ , (b)  $1.7 \times 10^{11}$ , (c)  $2.7 \times 10^{11}$ , and (d)  $3.8 \times 10^{11}$  W/cm<sup>2</sup>, respectively. The expansion of the laser-irradiated microdroplets changed drastically when the laser intensity was increased.

mismatch between the optimal laser spot size (295  $\mu\text{m}$ ) and droplet diameter (20  $\mu\text{m}$ ), the droplet must be expanded prior to laser irradiation by the main pulse. To achieve this we used instantaneous heating by a laser pre-pulse to expand a small microdroplet. In a previous study [27], a pre-pulse scheme was used to increase the density scale length of the plasma for enhancing the CE of x-ray radiation. In contrast, in this research, the main purpose of the laser pre-pulse is to expand the microdroplet.

The expansion behavior of pre-pulse irradiated Sn microdroplets was observed using a laser shadowgraph technique. The diameter of the droplets was 36  $\mu\text{m}$ , and the droplets were supported by a 6  $\mu\text{m}$ -diameter carbon fiber. The laser pre-pulse used to expand the droplets was the fundamental output of a Q-switched Nd:YAG laser. The pre-pulses were Gaussian with a pulse width of 8 ns and their intensities were in the range of  $5 \times 10^{10}$  to  $4 \times 10^{11}$  W/cm<sup>2</sup>. The second-harmonic of a Nd:YAG laser was used as the probe laser pulse (Gaussian with a 10-ns pulse width). The probe laser beam was perpendicular to the pre-pulse laser beam. The shadow of the laser-heated microdroplet was imaged using a gated CCD camera.

Figure 4 shows laser shadowgraphs of expanded droplets for various pre-pulse intensities. The artificial shadows indicate the initial position and shape of the droplets. The gate of the CCD camera was opened 0.5  $\mu\text{s}$  after the pre-pulse irradiation for a period of 10 ns. The expansion of the laser-heated droplet changed drastically when the laser intensity was increased and the expansion diameter approaches the optimal laser spot diameter. To expand the microdroplet, the intensity of the Nd:YAG laser pre-pulse must exceed  $3 \times 10^{11}$  W/cm<sup>2</sup>. The flying velocity of the expanded target was 0.5 - 1 km/s for  $2 - 4 \times 10^{11}$  W/cm<sup>2</sup>.

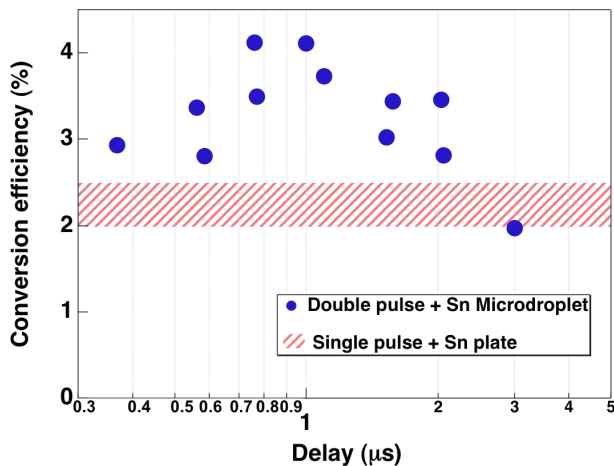


Fig. 5 Energy CEs of the main CO<sub>2</sub> laser beam to 13.5-nm-wavelength light within a 2% bandwidth. The CEs were measured by varying the temporal separation between the main CO<sub>2</sub> pulse and the Nd:YAG pre-pulse. An EUV-CE of 4% was attained by this scheme.

The expanded pure Sn droplet was irradiated with a CO<sub>2</sub> laser pulse. The incident angle of the pre-pulse was 20 degrees. from the incident axis of the CO<sub>2</sub> laser beam. The laser pre-pulse was the fundamental of a Q-switched Nd:YAG laser, whose output was a Gaussian with a pulse width of 8 ns, a focal spot size of 50 μm, and an intensity of  $4 \times 10^{11}$  W/cm<sup>2</sup>. The main laser pulses was from a CO<sub>2</sub> laser, and was Gaussian with a pulse width in the range 30 - 50 ns, a focal spot diameter of 250 μm, and an intensity of  $1 \times 10^{10}$  W/cm<sup>2</sup>. An in-band EUV microscope [28] coupled with a back-illuminated x-ray CCD camera was installed at 90 degrees with respect to the incident axis of the CO<sub>2</sub> laser beam.

The dependence of EUV-CE on the delay time between the pre-pulse and the main pulse is shown in Fig. 5. The EUV-CEs are in the range of 2.0 to 2.5 % for Sn plates irradiated with a single CO<sub>2</sub> pulse. This value is almost equal to that reported by Ueno *et al.* [26]. The highest CE (4%) was obtained for a delay of 1 μs. The dependence of the EUV-CE on laser intensity was also measured, and the optimal laser intensity was found to be  $1 \times 10^{10}$  W/cm<sup>2</sup> for a 1-μs delay.

Figure 6 shows (a) a laser shadowgraph of the expanded microdroplet taken 1 μs after the pre-pulse irradiation and (b) an in-band image of the CO<sub>2</sub>-laser-produced plasma. There are two EUV emission spots, one is caused by the tightly focused pre-pulse, and the other by the main CO<sub>2</sub> laser. The EUV emission region is located in the low-density region that is transparent to the probe light (wavelength of 0.53 μm). Based on a one-dimensional simulation, about half of the incident CO<sub>2</sub> laser energy is reflected by the surface of a Sn plasma in the single CO<sub>2</sub> laser irradiation case [29], because the density-scale-length is not sufficiently long to fully absorb the incident CO<sub>2</sub> laser en-

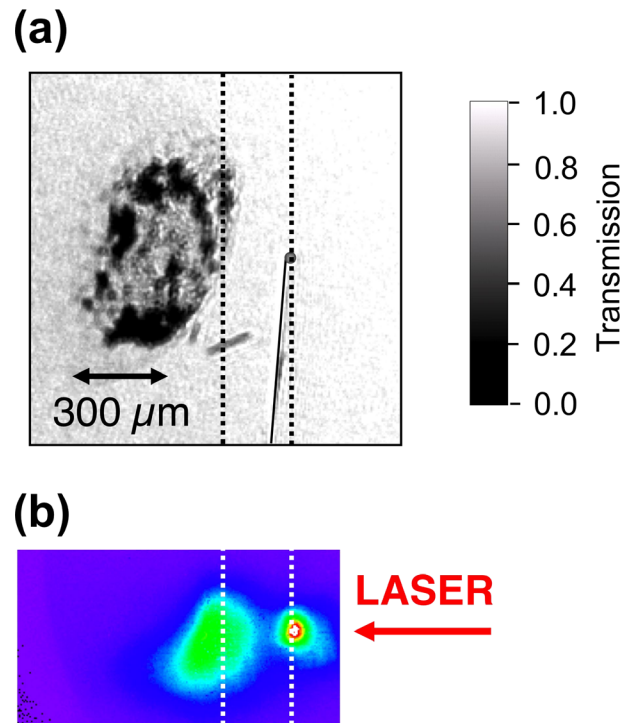


Fig. 6 (a) Side-on shadowgraph of an expanded microdroplet observed 1.0 μs after the laser pre-pulse irradiation when the CO<sub>2</sub> laser pulse irradiated the expanded microdroplet. (b) 13.5 nm in-band image of the produced plasma observed from the side. Both images have the same spatial scale.

ergy. The formation of low-density and long-scale-length targets by the pre-pulse irradiation enhances absorption of the CO<sub>2</sub> laser energy, resulting in a significant increase in the EUV-CE by 4%.

## 7. Design of a Practical EUV Light Source System

An example of a practical EUV light source system design is described. The droplet diameter is assumed to be 20 μm, the feasibility of which has been demonstrated at a repetition rate of 500 kHz [30, 31]. A Nd:YAG laser is selected to generate the pre-pulses. The intensity of the laser pre-pulses is  $4 \times 10^{11}$  W/cm<sup>2</sup>, the pulse width is 10 ns, the wavelength is 1.064 μm, and the spot diameter is 20 μm. Thus, the pre-pulse energy is 12.6 mJ/pulse and its power is 628 W. The intensity of the laser pre-pulse is sufficiently high to generate EUV light, and an EUV-CE of 1.5% was obtained in the above experiment. Thus, the EUV radiant energy due to pre-pulse irradiation is about 0.2 mJ/pulse. The residual radiant energy (10.7 mJ/pulse) must be generated by the main CO<sub>2</sub> laser irradiation. The intensity of the main pulse is  $1 \times 10^{10}$  W/cm<sup>2</sup>, the pulse width is 40 ns, and the EUV-CE was 4%. Thus, the laser energy is 268 mJ/pulse and the spot size is 292 μm. In this manner, a practical EUV light source can be designed with a 50 kHz-

0.63 kW Nd:YAG laser system and a 50 kHz-13.4 kW CO<sub>2</sub> using a 20- $\mu$ m-diameter droplet. The total EUV-CE of the system is calculated to be 3.9%. This design may minimize the amount of debris and OOB radiation.

## 8. Summary

EUV light is mainly generated from Sn atoms located within a depth of 10 nm from the target surface in the laser spot. The region deeper than 10 nm and its periphery are the source of the neutral debris and OOB radiation. The minimum-mass Sn target is the essential solution to minimize amount of the neutral debris and OOB radiation. Using the minimum-mass target makes reduces the amounts of neutral debris and OOB radiation to be reduced by less than 1.4% and 24%, respectively, compared to those for bulk targets. CO<sub>2</sub> laser rather than Nd:YAG laser is a preferable driver owing to not only high EUV-CE but also low emission of neutral debris and OOB radiation. The number of in-band photons emitted per a Sn ion was measured to be in the range of 5 to 10. A pure Sn microdroplet containing the minimum-mass Sn atoms ( $7.4 \times 10^{13}$  -  $1.5 \times 10^{14}$ ) is one of the practical targets because it is suitable for continuous supply of the Sn fuel. Laser-pre-pulse-driven expansion of pure Sn microdroplet is demonstrated to solve the considerable mismatch between the optimal laser spot diameter (300  $\mu$ m) and the diameter (20  $\mu$ m) of the minimum-mass microdroplets. The formation of low-density and long-scale-length targets by the pre-pulse irradiation enhances absorption of the CO<sub>2</sub> laser energy, resulting in a significant increase in the EUV-CE by 4%. A 180 W EUV light source system is achievable with a 50 kHz-0.63 kW Nd:YAG laser of the pre-pulse and 50 kHz-13.4 kW CO<sub>2</sub> laser of the main pulse.

## Acknowledgement

This work was performed under the auspices of a Leading Project and Grant-in-Aid for Young Scientists (A) (Grant No. 21684034) promoted by the Japanese Ministry of Education, Culture, Sports, Science and Technology (MEXT). We thank H. Tanuma, S. Namba, T. Aota, N. Ozaki, T. Ando, M. Shimomura, H. Sakaguchi, S. Maeda, and Y. Nakai for their great contributions to this work.

- [1] V. Bakshi, ed., *EUV Sources for Lithography* (SPIE Press, Bellingham, WA, 2005), ISBN 0-8194-5845-7.
- [2] R.C. Spitzer, T.J. Orzechowski, D.W. Phillion, R.L. Kauffman and C. Cerjan, *J. Appl. Phys.* **79**, 2251 (1996).
- [3] M. Richardson, G.-S. Koay, K. Takenoshita, C. Keyser and M. Al-Rabban, *J. Vac. Sci. Technol. B* **22**, 785 (2004).
- [4] Y. Shimada, H. Nishimura, M. Nakai, K. Hashimoto, M. Yamaura, Y. Tao, K. Shigemori, T. Okuno, K. Nishihara, T. Kawamura *et al.*, *Appl. Phys. Lett.* **86**, 051501 (2005).
- [5] S. Fujioka, H. Nishimura, K. Nishihara, A. Sasaki, A. Sunahara, T. Okuno, N. Ueda, T. Ando, Y. Tao, Y. Shimada *et al.*, *Phys. Rev. Lett.* **95**, 235004 (2005).
- [6] H. Tanaka, A. Matsumoto, K. Akinaga, A. Takahashi and T. Okada, *Appl. Phys. Lett.* **87**, 041503 (2005).
- [7] K. Nishihara, A. Sasaki, A. Sunahara and T. Nishikawa, *EUV Sources for Lithography* (SPIE Press, 2006), vol. PM149, chap.11, p.339.
- [8] T. Ando, S. Fujioka, H. Nishimura, T. Aota, N. Ueda, M. Shimomura, H. Sakaguchi, Y. Yasuda, K. Nagai, T. Norimatsu *et al.*, *Appl. Phys. Lett.* **89**, 151501 (2006).
- [9] J. White, G. O'Sullivan, S. Zakharov, P. Choi, V. Zakharov, H. Nishimura, S. Fujioka and K. Nishihara, *Appl. Phys. Lett.* **92**, 151501 (2008).
- [10] S. Fujioka, H. Nishimura, K. Nishihara, Y.-G. Kang, Y. Shimada, A. Sunahara, H. Furukawa, Q. Gu, K. Nagai, T. Norimatsu *et al.*, *Appl. Phys. Lett.* **87**, 241503 (2005).
- [11] S. Namba, S. Fujioka, H. Nishimura, Y. Yasuda, K. Nagai, N. Miyanaga, Y. Izawa, K. Mima and K. Takiyama, *Appl. Phys. Lett.* **88**, 171503 (2006).
- [12] M. Shimomura, S. Fujioka, T. Ando, H. Sakaguchi, Y. Nakai, Y. Yasuda, H. Nishimura, K. Nagai, T. Norimatsu, K. Nishihara *et al.*, *Appl. Phys. Express* **1**, 056001 (2008).
- [13] H. Tanaka, Y. Hashimoto, K. Tamaru, A. Takahashi and T. Okada, *Appl. Phys. Lett.* **89**, 181109 (2006).
- [14] H. Sakaguchi, S. Fujioka, S. Namba, H. Tanuma, H. Ohashi, S. Suda, M. Shimomura, Y. Nakai, Y. Kimura, Y. Yasuda *et al.*, *Appl. Phys. Lett.* **92**, 111503 (2008).
- [15] S. Namba, S. Fujioka, H. Sakaguchi, H. Nishimura, Y. Yasuda, K. Nagai, N. Miyanaga, Y. Izawa, K. Mima, K. Sato *et al.*, *J. Appl. Phys.* **104**, 013305 (2008).
- [16] S. Fujioka, M. Shimomura, Y. Shimada, S. Maeda, H. Sakaguchi, Y. Nakai, T. Aota, H. Nishimura, N. Ozaki, A. Sunahara *et al.*, *Appl. Phys. Lett.* **92**, 241502 (2008).
- [17] F. Bijkerk, G. Hergenhan, G. Schriever, K. Gabel, M. Schuermann, R. de Bruijn, S.A.V.D. Westen, T. Missalla, U. Stamm and V. Bakshi, Tech. Rep. 04024498A-TR, International SEMATECH Manufacturing Initiative (2004).
- [18] R.A. Stern and J.A.J. III, *Phys. Rev. Lett.* **34**, 0015048 (1975).
- [19] T. Ando, S. Fujioka, Y. Shimada, T. Birou, S. Maeda, Y. Yasuda, K. Nagai, T. Norimatsu, H. Nishimura, K. Nishihara *et al.*, *Jpn. J. Appl. Phys.* **47**, 293 (2008).
- [20] H. Over, Y.B. He, A. Farkas, G. Mellau, C. Korte, M. Knapp, M. Chandhok and M. Fang, *J. Vac. Sci. Tech. B* **25**, 1123 (2007).
- [21] P. Dunne, O. Morris, E. Sokell, F. O'Reilly, G. O'Sullivan, N. Murphy and P. Hayden, Tech. Rep., SEMATECH (2006).
- [22] O. Morris, P. Hayden, F. O'Reilly, N. Murphy, P. Dunne and V. Bakshi, *Appl. Phys. Lett.* **91**, 081506 (2007).
- [23] J.A. Koch, O.L. Landen, T.W. Barbee, J.P. Celliers, L.B.D. Silva, S.G. Glendinning, B.A. Hammel, D.H. Kalantar and C.B.J. Seely, *Appl. Opt.* **37**, 1784 (1998).
- [24] N.M. Ceglio, R.L. Kauffman, A.M. Hawryluk and H. Medeck, *Appl. Opt.* **22**, 318 (1983).
- [25] L. Poletto, A. Boscolo and G. Tondello, *Appl. Opt.* **38**, 29 (1999).
- [26] Y. Ueno, G. Soumagne, A. Sumitani, A. Endo and T. Higashiguchi, *Appl. Phys. Lett.* **91**, 231501 (2007).
- [27] R. Kodama, T. Mochizuki, K.A. Tanaka and C. Yamanaka, *Appl. Phys. Lett.* **50**, 720 (1987).
- [28] Y. Tao, M. Nakai, H. Nishimura, S. Fujioka, T. Okuno, T. Fujiwara, N. Ueda, N. Miyanaga and Y. Izawa, *Rev. Sci. Instrum.* **75**, 5173 (2005).
- [29] K. Nishihara, A. Sunahara, A. Sasaki, M. Nunami, H. Tanuma, S. Fujioka, Y. Shimada, K. Fujima, H. Furukawa, T. Kato *et al.*, *Phys. Plasmas* **15**, 056708 (2008).

- [30] A. Endo, H. Hoshino, T. Sukanuma, K. Nowak, T. Yamagida, T. Yabu, T. Asayama, Y. Ueno, M. Moriya, M. Nakano *et al.*, in *2007 International EUVL Symposium* (Sapporo, Japan, 2007), p.SO-07.
- [31] D.C. Brandt, I.V. Fomenkov, N.R. Bowering, A.I. Ershov, W.N. Partlo, D.W. Myers, G.O. Vaschnko, O.V. Khodykin, A.N. Bykanov, J.R. Hoffman *et al.*, in *2007 International EUVL Symposium* (Sapporo, Japan, 2007), p.SO-06.